Mechanics of Advanced Composite Structures 2 (2015) 135-144

Semnan University

Mechanics of Advanced Composite Structures

journal homepage: http://macs.journals.semnan.ac.ir

# Buckling Analysis of Spherical Composite Panels Reinforced by Carbon Nanotube

**S. Pouresmaeeli, S.A. Fazelzadeh*, E. Ghavanloo**

*School of Mechanical Engineering, Shiraz University, Shiraz, Iran*

**PAPER INFO**

***Paper history:***
Received 22 November 2015
Received in revised form 9 February 2016
Accepted 29 February 2016

***Keywords:***
Buckling
Carbon nanotube-reinforced
Nanocomposite
Spherical panel

**ABSTRACT**

In this study, the buckling behavior of moderately thick Carbon Nano-Tube (CNT)-reinforced spherical composite panels subjected to both uniaxial and biaxial loads is examined. The uniform and various kinds of functionally graded distributions of the CNT are considered. The mechanical properties of the nanocomposite panels are estimated using the modified rule of mixture. Based on the first-order shear deformation theory and the von Karman-type of kinematic nonlinearity, the governing differential equations are derived and the solutions are determined using Galerkin's method. The suggested model is justified by a good agreement between the present results and those reportedin the literature. The numerical results are performed to elucidate the influences of volume fraction, aspect ratio, thickness ratio and side-to-radius ratio on the critical buckling loads of the spherical nanocomposite panels. One of the main contributions of the current study is to investigate the effectiveness of functionally graded distributions.The effectiveness of functionally graded distributions with respect to various parameters are also investigated.



## 1. Introduction

In recent decades, the composite materials have found numerous applications in various weight sensitive industries such as aviation, automobile and marine industries. Fiber reinforced composite, a widespread kind of composite material, is constituted by fibers as reinforcement and a polymer matrix as a load transfer medium. As a result of low costs, tailorable characteristics, high strength and stiffness to weight ratios, fiber reinforced composites have attracted great attentions. In 1991, Iijima [1] discovered Carbon Nano-Tube (CNT) as a novel nanostructure with outstanding mechanical, thermal and electrical properties. The emergence of carbon nanotubes has received relatively great consideration and consequently they were introduced as a novel candidate for reinforcing polymer matrices replacing the conventional reinforcements [2–5]. Researches on the properties of composites reinforced by CNT demonstrate that adding only 1%weight fraction of CNTs results in a 36-42 percent increase inelastic modulus, 150 percent increase in strain energy density and25percent increase in tensile strength [6, 7]. Therefore, adding CNTs into the matrix reveals significant improvement in their mechanical properties. Hence, substantial investigations have been carried out topredict the physical properties and to investigate mechanical behaviorof Carbon Nanotube-Reinforced Composites (CNTRC) [8-11].

Since the critical buckling load is a key factor in designing of shell structural elements, the static instability of nanocomposite panels becomes the subject of primary interest in recent studies [12-19]. Shen [12-14, 17] investigated the static stabilities of CNTRC cylindrical shells in thermal environments. The higher-order shear deformation theory with thevon Karman-type of kinematic nonlinearity was used to derive differential governing equations of Functionally Graded Carbon Nanotube-Reinforced Composites (FG-CNTRC). In his works, the buckling,

*Corresponding author, Tel.: +98-71-36133238, Fax: +98-71-36473511

*E-mail address: fazelzad@shirazu.ac.ir*

postbuckling and thermal buckling of CNTRC cylindrical shells subjected to axial compression load, pressure and torsion loads were analyzed. In addition, perfect and imperfect CNTRC cylindrical shells were taken into consideration. Using meshless approach, Liew et al. [16] examined the postbuckling of theFG-CNTRC cylindrical panels under axial compression. Furthermore, applying a two-step perturbation approach, the postbuckling of temperature-dependent CNTRC cylindrical panel resting on theelastic foundations and subjected to axial compression was investigated by Shen and Xiang [18]. Jam and Kiani [19] analysed the buckling of the FG-CNTRC conical shells subjected to lateral pressure. The numerical results were obtained using the trigonometric functions in circumferential direction and using the generalized differential quadrature method in axial direction.Recently, Rabani Bidgoliet al. [20] investigated the nonlinear vibration and instability of CNT reinforced cylindrical shell conveying viscous fluid. The nanocomposite is resting on orthotropic Pasternak medium and the material properties of nanocomposites are predicted using the rule of mixture.

As a result of the potential applications of nanocomposites in Nano-Electro-Mechanical Systems (NEMS) and Micro-Electro-Mechanical Systems (MEMS), the instability of CNT reinforced microplate has been analyzed recently [21-24]. Mohammadimehr et al. [22] studied the biaxial buckling and bending of the double-coupled plates reinforced by boron nitride nanotubes and CNT using the modified strain gradient. The buckling, bending and free vibration of CNT reinforced microplate subjected to hydro-thermal environments were examined using differential quadrature method [23]. Ghorbanpour Arani et al. [24] investigated the wave propagation of CNT reinforced piezoelectric microplates under the longitudinal magnetic and three-dimensional electric fields.

Despite the considerable number of investigations in the area of stability of the CNTRC panels, the buckling analysis of CNTRC spherical panel is not investigated. The main purpose of this research is to predict the critical uniaxial and biaxial buckling load of the moderately thick CNTRC spherical panel. In addition, new parameter percent change of buckling load is defined to examine the effectiveness of functionally graded distributions of CNTs on the critical buckling loads.

The effective material properties of nanocomposite panelsare estimated based on the modified rule of mixture.

The differential governing equations of CNTRC are derived on the basis of the first-order shear deformation theory and the von Karman-type of kinematic nonlinearity. Moreover, the non-dimensional uniaxial and biaxial buckling loads are obtained utilizing Galerkin's method. The accuracy of the presented results is validated with those found in the literature. Furthermore, the effects of aspect ratio, volume fraction of CNTs, thickness ratio and side-to-radius ratio are elucidated and the effectiveness of functionally graded distributions in buckling behavior of CNTRC is investigated.

## 2. Theory and Formulations

A CNTRC spherical panel with the length $a$, width $b$, thickness $h$ and radius of curvature $R$is shown in Fig. 1. An orthogonal curvilinear coordinate system ($x$,$y$,$z$) is established on the middle surface of the panel. The carbon nanotube-reinforced composite is made of a mixture of a polymer matrix and single-walled CNTs as reinforcements. The reinforcements can be randomly distributed or uniaxially aligned in the matrix. Due tothe dispersion and agglomeration challenges, the volume fraction of the CNTsis restricted. As a result ofthis limitation, the distributions of the CNTs can be functionally graded in thickness of panels [25].

In this study, CNTs are assumed to be uniaxially aligned in $x$ direction. Furthermore, the uniform distributions (UDs) of the CNTs in the thickness of the panel and four types of functionally graded distributions well-knownas FG-A, FG-V, FG-O and FG-X are considered (Fig. 2). In the case of FG-A contrary to FG-V, the bottom surface of panel is CNT-rich. In addition, in FG-X case, the bottom and top surfaces of panel are CNT-rich, contrary to FG-O.

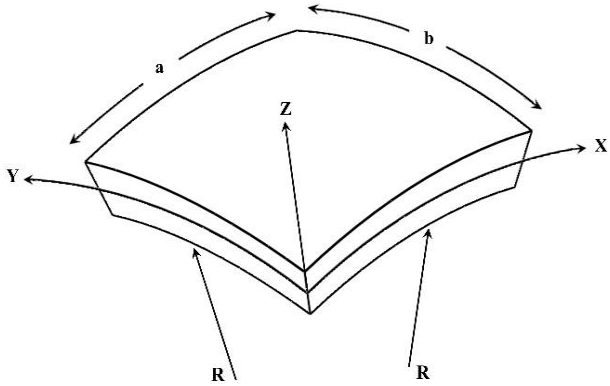


**Figure 1.** The geometrical dimensions of spherical panels

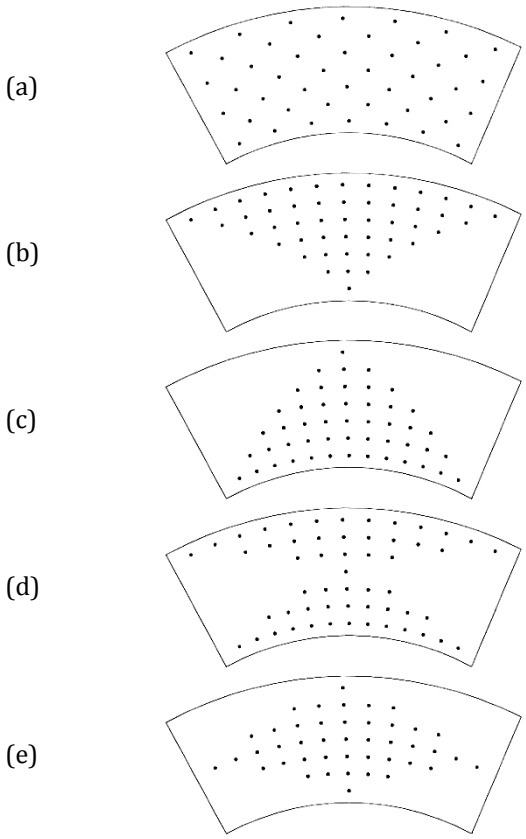


**Figure 2.** The configurations of the UD and FG-CNTRC panels (a) UD; (b) FG-V; (c) FG-A; (d) FG-X; (e) FG-O

The CNT volume fraction of these five types are defined as what follows [26]:

$$\begin{aligned}
&\text{UD: } V_{CNT} = V_{CNT}^{*} \\
&\text{FG-A: } V_{CNT}(z) = (1-2z/h)V_{CNT}^{*} \\
&\text{FG-V: } V_{CNT}(z) = (1+2z/h)V_{CNT}^{*} \\
&\text{FG-X: } V_{CNT}(z) = (4|z|/h)V_{CNT}^{*} \\
&\text{FG-O: } V_{CNT}(z) = 2(1-2|z|/h)V_{CNT}^{*}
\end{aligned} \tag{1}$$

where $V_{CNT}^{*}$ indicates the overall CNT volume fractions and is defined as follows:

$$V_{CNT}^{*} = \frac{w_{CNT}}{w_{CNT} + (\rho^{CNT}/\rho^{m})(1-w_{CNT})} \tag{2}$$

where $w_{\mathrm{CNT}}$ is the mass fraction of the CNTs. $\rho^{\mathrm{m}}$ and $\rho^{\mathrm{CNT}}$ denote the densities of the matrix and CNTs, respectively. To predict the effective material properties of CNTRC, the modified rule of mixture can be expressed as what follows [27]:

$$\begin{aligned}
&E_{11}(z) = \eta_1 V_{CNT}(z) E_{11}^{CNT} + V_m(z) E^{m} \\
&\frac{\eta_2}{E_{22}(z)} = \frac{V_{CNT}(z)}{E_{22}^{CNT}} + \frac{V_m(z)}{E^{m}} \\
&\frac{\eta_3}{G_{12}(z)} = \frac{V_{CNT}(z)}{G_{12}^{CNT}} + \frac{V_m(z)}{G^{m}} \\
&\nu_{12} = V_{CNT}^{*}\,\nu_{12}^{CNT} + (1-V_{CNT}^{*})\nu^{m}
\end{aligned} \tag{3}$$

where $E_{11}$, $E_{22}$ and $G_{12}$ are the mechanical properties of the CNTRCs. $E^{\mathrm{m}}$ and $G^{\mathrm{m}}$ represent Young's moduli and shear moduli of the matrix, respectively. In addition, $E_{11}^{CNT}$, $E_{22}^{CNT}$ and $G_{12}^{CNT}$ represent Young's and shear moduli of the CNTs. Furthermore, $V_{\mathrm{CNT}}$ and $V_{\mathrm{m}}$ are the volume fractions of the CNTs and matrix, respectively.

It is well known that the load transfer between the nanotubes and the matrix is not perfect. Therefore, several effects including size and surface effects must be considered. In order to incorporate these effects, the modified rule of mixture is usually used and so CNT efficiency parameters ($\eta_1$, $\eta_2$ and $\eta_3$) are introduced. According to this point, application of the size dependent continuum theories such as the modified couple stress theory, strain gradient theory etc. is not necessary [20]. To calculate the value of the CNT efficiency parameters, the elastic modulus of the CNTRCs predicted by the molecular dynamics simulations should be matched with those determined from the rule of mixture.

Here, the CNTRC spherical panels are assumed to be moderately thick and they are modelled by the first-order shear deformation theory [28]. In this study, $z/R$ in comparison with unityis neglectedand the von Karman-type of kinematic nonlinearity is considered.

For spherical nanocompositepanels, strain-displacement relations are expressed as what follows [28]:

$$\begin{aligned}
&\varepsilon_{xx} = \frac{\partial u}{\partial x} + \frac{w}{R} + z\frac{\partial \varphi_x}{\partial x} + \frac{1}{2}\left(\frac{\partial w}{\partial x}\right)^2 \\
&\varepsilon_{yy} = \frac{\partial v}{\partial y} + \frac{w}{R} + z\frac{\partial \varphi_y}{\partial y} + \frac{1}{2}\left(\frac{\partial w}{\partial y}\right)^2 \\
&\gamma_{xy} = \frac{\partial u}{\partial y} + \frac{\partial v}{\partial x} + z\left[\frac{\partial \varphi_x}{\partial y} + \frac{\partial \varphi_y}{\partial x}\right] + \frac{\partial w}{\partial x}\frac{\partial w}{\partial y} \\
&\gamma_{xz} = \varphi_x + \frac{\partial w}{\partial x} - \frac{u}{R} \\
&\gamma_{yz} = \varphi_y + \frac{\partial w}{\partial y} - \frac{v}{R}
\end{aligned} \tag{4}$$

where $\varepsilon$ and $\gamma$ are the normal and shear strains, respectively. In addition, $u$, $v$ and $w$ indicate displacements of the mid-surface along $x$, $y$ and $z$ directions, respectively. Also, $\varphi_{\mathrm{x}}$ and $\varphi_{\mathrm{y}}$ are rotations of normal to the mid-surface about the $y$ and $x$ axes, respectively. The terms $\frac{1}{2}(\partial w/\partial x)^2$, $\frac{1}{2}(\partial w/\partial y)^2$ and $\partial w/\partial x\,\partial w/\partial y$ are the von Karman terms.

Applying the Hamilton's principle, one can obtain the equilibrium equations of the CNTRC spherical panels as follows [28]:

$$\frac{\partial N_{xx}}{\partial x} + \frac{\partial N_{xy}}{\partial y} + \frac{Q_{xz}}{R_x} = 0 \tag{5}$$

$$\frac{\partial N_{yy}}{\partial y}+\frac{\partial N_{xy}}{\partial x}+\frac{Q_{yz}}{R_y}=0$$

$$\frac{N_{xx}}{R_x}+\frac{N_{yy}}{R_y}-\frac{\partial Q_{xz}}{\partial x}-\frac{\partial Q_{yz}}{\partial y}=\hat{N}_x\frac{\partial^2 w}{\partial x^2}+\hat{N}_y\frac{\partial^2 w}{\partial y^2}$$

$$\frac{\partial M_{xx}}{\partial x}+\frac{\partial M_{xy}}{\partial y}-Q_{xz}=0$$

$$\frac{\partial M_{yy}}{\partial y}+\frac{\partial M_{xy}}{\partial x}-Q_{yz}=0$$

where $N_{xx}$, $N_{yy}$ and $N_{xy}$arethe in-plane stress resultants and $M_{xx}$, $M_{yy}$ and $M_{xy}$ are the stress couple resultants. Furthermore, $Q_{xz}$ and $Q_{yz}$ are the transverse shear stress resultants.

Furthermore, $\hat{N}_x$ and $\hat{N}_y$ are thein-plane distributed forces in the $x$ and $y$ directions, respectively. The stress resultants can be defined as what follows [25]:

$$\{N_{xx},N_{yy},N_{xy}\}=\int_{-\frac{h}{2}}^{\frac{h}{2}}\{\sigma_{xx},\sigma_{yy},\tau_{xy}\}dz$$

$$\{M_{xx},M_{yy},M_{xy}\}=\int_{-\frac{h}{2}}^{\frac{h}{2}}\{z\sigma_{xx},z\sigma_{yy},z\tau_{xy}\}dz \tag{6}$$

$$\{Q_{xz},Q_{yz}\}=k_s\int_{-\frac{h}{2}}^{\frac{h}{2}}\{\tau_{xz},\tau_{yz}\}dz$$

where $k_s$ is the shear correction factor and is equal to 5/6 [29].

It is shown that uniaxially aligned CNTRCs reveal orthotropic characteristics [13, 16].Thus, the stress–strain relations are defined as what follows [26]:

$$\begin{pmatrix}\sigma_{xx}\\ \sigma_{yy}\\ \tau_{yz}\\ \tau_{xz}\\ \tau_{xy}\end{pmatrix}=\begin{bmatrix}\frac{E_{11}}{1-\nu_{12}\nu_{21}} & \frac{\nu_{12}E_{22}}{1-\nu_{12}\nu_{21}} & 0 & 0 & 0\\ \frac{\nu_{12}E_{22}}{1-\nu_{12}\nu_{21}} & \frac{E_{22}}{1-\nu_{12}\nu_{21}} & 0 & 0 & 0\\ 0 & 0 & G_{23} & 0 & 0\\ 0 & 0 & 0 & G_{13} & 0\\ 0 & 0 & 0 & 0 & G_{12}\end{bmatrix}\begin{pmatrix}\varepsilon_{xx}\\ \varepsilon_{yy}\\ \gamma_{yz}\\ \gamma_{xz}\\ \gamma_{xy}\end{pmatrix} \tag{7}$$

Substituting Eq. (4), (6) and (7) into Eq. (5), the governing differential equations as functions of the mid-surface displacements and rotations can be obtained as what follows:

$$A_1\frac{\partial^2 u}{\partial x^2}+C_1\frac{\partial^2 u}{\partial y^2}+(\nu_{12}B_1+C_1)\frac{\partial^2 v}{\partial x\partial y}+A_2\frac{\partial^2\varphi_x}{\partial x^2}$$
$$+\frac{k_sF_1}{R}(\varphi_x-\frac{u}{R})+C_2\frac{\partial^2\varphi_x}{\partial y^2}+(\nu_{12}B_2+C_2)\frac{\partial^2\varphi_y}{\partial x\partial y} \tag{8}$$
$$+(\frac{A_1+\nu_{12}B_1+k_sF_1}{R})\frac{\partial w}{\partial x}=0$$

$$B_1\frac{\partial^2 v}{\partial y^2}+C_1\frac{\partial^2 v}{\partial x^2}+(\nu_{12}B_1+C_1)\frac{\partial^2 u}{\partial x\partial y}+B_2\frac{\partial^2\varphi_y}{\partial y^2}$$
$$+\frac{k_sD_1}{R}(\varphi_y-\frac{v}{R})+C_2\frac{\partial^2\varphi_y}{\partial x^2}+(\nu_{12}B_2+C_2)\frac{\partial^2\varphi_x}{\partial x\partial y} \tag{9}$$
$$+(\frac{B_1+\nu_{12}B_1+k_sD_1}{R})\frac{\partial w}{\partial y}=0$$

$$(\frac{A_1+\nu_{12}B_1+k_sF_1}{R})\frac{\partial u}{\partial x}+(\frac{B_1+\nu_{12}B_1+k_sD_1}{R})\frac{\partial v}{\partial y}$$
$$+(\frac{A_2+\nu_{12}B_2}{R}-k_sF_1)\frac{\partial\varphi_x}{\partial x}-(k_sF_1+\hat{N}_x)\frac{\partial^2 w}{\partial x^2}$$
$$+(\frac{B_2(1+\nu_{12})}{R}-k_sD_1)\frac{\partial\varphi_y}{\partial y}-(k_sD_1+\hat{N}_xS_y)\frac{\partial^2 w}{\partial y^2} \tag{10}$$
$$+(\frac{A_1+(1+2\nu_{12})B_1}{R^2})w=0$$

$$A_2\frac{\partial^2 u}{\partial x^2}+C_2\frac{\partial^2 u}{\partial y^2}+(\nu_{12}B_2+C_2)\frac{\partial^2 v}{\partial x\partial y}+A_3\frac{\partial^2\varphi_x}{\partial x^2}$$
$$+C_3\frac{\partial^2\varphi_x}{\partial y^2}+(\nu_{12}B_3+C_3)\frac{\partial^2\varphi_y}{\partial x\partial y}-k_sF_1(\varphi_x-\frac{u}{R}) \tag{11}$$
$$+(\frac{A_2+\nu_{12}B_2}{R}-k_sF_1)\frac{\partial w}{\partial x}=0$$

$$B_2\frac{\partial^2 v}{\partial y^2}+C_2\frac{\partial^2 v}{\partial x^2}+(\nu_{12}B_2+C_2)\frac{\partial^2 u}{\partial x\partial y}+C_3\frac{\partial^2\varphi_y}{\partial x^2}$$
$$+B_3\frac{\partial^2\varphi_y}{\partial y^2}+(\nu_{12}B_3+C_3)\frac{\partial^2\varphi_x}{\partial x\partial y}-k_sD_1(\varphi_y-\frac{v}{R}) \tag{12}$$
$$+(\frac{(1+\nu_{12})B_2}{R}-k_sD_1)\frac{\partial w}{\partial y}=0$$

where $S_y$ is denoted as $\hat{N}_y/\hat{N}_x$ and,$A_i$, $B_i$, $C_i$, $D_1$ and $F_1$ ($i$=1, 2, 3) are defined by the following equations:

$$\{A_1,A_2,A_3\}=\int_{-h/2}^{h/2}\left(\frac{E_{11}}{(1-\nu_{12}\nu_{21})}\right)\{1,z,z^2\}dz$$

$$\{B_1,B_2,B_3\}=\int_{-h/2}^{h/2}\left(\frac{E_{22}}{(1-\nu_{12}\nu_{21})}\right)\{1,z,z^2\}dz \tag{13}$$

$$\{C_1\quad C_2\quad C_3\}=\int_{-h/2}^{h/2}G_{12}\{1\quad z\quad z^2\}dz$$

$$\{D_1\quad F_1\}=\int_{-h/2}^{h/2}\{G_{23}\quad G_{13}\}dz$$

Here, amovable simply supported boundary condition is considered. To solve the complex and highly-coupled governing differential equations, the displacement field is estimated utilizing sets of trigonometric expansions, as follows:

$$u=\mathbf{\Phi}_u^T\mathbf{q}_u=\sum_{m=1}^{m'}\sum_{n=1}^{n'}q_{u_{mn}}\cos\left(\frac{m\pi x}{a}\right)\sin\left(\frac{n\pi y}{b}\right)$$

$$v=\mathbf{\Phi}_v^T\mathbf{q}_v=\sum_{m=1}^{m'}\sum_{n=1}^{n'}q_{v_{mn}}\sin\left(\frac{m\pi x}{a}\right)\cos\left(\frac{n\pi y}{b}\right)$$

$$w=\mathbf{\Phi}_w^T\mathbf{q}_w=\sum_{m=1}^{m'}\sum_{n=1}^{n'}q_{w_{mn}}\sin\left(\frac{m\pi x}{a}\right)\sin\left(\frac{n\pi y}{b}\right)$$
$$\varphi_x=\mathbf{\Phi}_x^T\mathbf{q}_x=\sum_{m=1}^{m'}\sum_{n=1}^{n'}q_{x_{mn}}\cos\left(\frac{m\pi x}{a}\right)\sin\left(\frac{n\pi y}{b}\right)$$
$$\varphi_y=\mathbf{\Phi}_y^T\mathbf{q}_y=\sum_{m=1}^{m'}\sum_{n=1}^{n'}q_{y_{mn}}\sin\left(\frac{m\pi x}{a}\right)\cos\left(\frac{n\pi y}{b}\right) \quad (14)$$

where $\mathbf{q}_u$, $\mathbf{q}_v$, $\mathbf{q}_w$, $\mathbf{q}_x$ and $\mathbf{q}_y$ are the vectors of generalized coordinates and $\mathbf{\Phi}_u$, $\mathbf{\Phi}_v$, $\mathbf{\Phi}_w$, $\mathbf{\Phi}_x$ and $\mathbf{\Phi}_y$ are the shape functions. Moreover, $m'$ and $n'$ are the number of modes.Hence, applying the Galerkin's method, the governing equations can be simplified as the following equations:

$$\left(\mathbf{K}-\hat{N}_x\mathbf{L}\right)\mathbf{q}=0 \quad (15)$$

Where $\mathbf{q}$ is the overall vector of the generalized coordinates defined as follows:

$$\{\mathbf{q}\}=\left\{\mathbf{q}_u^T\quad\mathbf{q}_v^T\quad\mathbf{q}_w^T\quad\mathbf{q}_x^T\quad\mathbf{q}_y^T\right\}^T \quad (16)$$

Thus, determining the eigenvalue problem of Eq. (15), the critical buckling loadof the CNTRC spherical panels can be computed. For parametric studies, the non-dimensional critical buckling load is defined as what follows:

$$N_{cr}=\frac{\hat{N}_x a^2}{E^m h^3} \quad (17)$$

To assess the effectiveness of the functionally graded distributions in comparison with the uniform distribution of CNTson the critical buckling loads, a new parameter entitled percentage change of critical buckling loads, PCB, is defined as follow

$$\mathrm{PCB}=\left(\frac{\left(N_{cr}^{FG}-N_{cr}^{UD}\right)}{N_{cr}^{UD}}\right)*100 \quad (18)$$

Where $N_{cr}^{FG}$ and $N_{cr}^{UD}$ are the non-dimensional critical loads ofthe functionally graded and uniformly distributed nanocomposite, respectively.

## 3. Results and Discussion

In order to confirm the accuracy of the present results, the non-dimensional critical loads of functionally graded square spherical shell and plate are compared with those available in the literature [30]. The material properties used to validate the results are what follow [30]:

Metal (Aluminium, Al):

$E_m=70\times10^9\ \mathrm{N/m^2}, \nu=0.3, \rho_m=2702\mathrm{kg/m^3}$

Ceramic (Alumina, $Al_2O_3$):

$E_c=38\times10^{10}\ \mathrm{N/m^2}, \nu=0.3, \rho_c=3800\mathrm{kg/m^3}$

The results are presented in Table 1 and the precision of the current procedure is verified. In this study, poly {(m-phenylenevinylene)-co-[(2,5-dioctoxy-p-phenylene) vinyl-ene]} well-known as PmPV and (10, 10) single-walled CNTsare considered as the polymer matrix and reinforcements, respectively. The mechanical properties of the matrix andthe CNTs are listedin Table 2. TheCNTs efficiency parametersare taken as $\eta_1 = 0.149$ and $\eta_2 = 0.934$ for $V^*_{CNT} = 0.11$, $\eta_1 = 0.150$ and $\eta_2 = 0.941$ for $V^*_{CNT} = 0.14$. Furthermore, $\eta_1 = 0.149$ and $\eta_2 = 1.381$ for $V^*_{CNT} = 0.17$, additionally, $\eta_3 = \eta_2$ [25].

To reveal the effect of volume fraction, non-dimensional critical buckling loads for various volume fractions are computed and givenin Table 3. It is shown that with the increase in the CNT volume fraction, the stiffness of CNTRC spherical panel increases and consequently, the non-dimensional critical uniaxial and biaxial loads increase. Furthermore, the influence of volume fraction on the uniaxial buckling loads of FG-X nanocomposite panel with respect to aspect ratio, $a/b$, is depicted in Fig. 3. Here, it takes $h/a = 0.05$ and $a/R = 0.5$. It demonstrates the same physical phenomena as presented in Table 3 and the uniaxial buckling loads increase by increasing the aspect ratio.

Figs. 4 and 5 reveal the influence of the aspect ratio on the non-dimensional critical uniaxial and biaxial loads, respectively. Here, it takes $V^*_{\mathrm{CNT}} = 0.11$, $h/a = 0.05$ and $a/R = 0.5$. It is shown that by increasing the aspect ratio, the uniaxial buckling load increases extremely. It is noticed that the similar trend for buckling of nanocomposite plate is mentioned in Ref. [31]. However, the non-dimensional critical biaxial loads vary non-monotonically with the increase of the aspect ratio. As it is expected, the CNTRC spherical panels under the uniaxial loads are more stable than the CNTRC panels subjected to biaxial loads.

**Table 1.** The comparisons of the critical loads of functionally graded sphericalpanel and plate ( $N_{cr}=\hat{N}_x/E_c h$ )

| $\frac{a}{R}$ | | Power law index | | | |
|---|---|---|---|---|---|
| | | $k=0$ | $k=0.5$ | $k=4$ | $k=\infty$ |
| 0 | Ref. [30] | 0.03381 | 0.02214 | 0.01131 | 0.00623 |
| | Present study | 0.03422 | 0.02231 | 0.01160 | 0.00638 |
| 0.5 | Ref. [30] | 0.05720 | 0.03952 | 0.01973 | 0.01054 |
| | Present study | 0.05440 | 0.03599 | 0.01830 | 0.01013 |

**Table 2.** The mechanical properties of the PmPV and CNTs [25]

| | | | | |
|---|---|---|---|---|
| CNTs | $E_{11}$ | $E_{22}$ | $G_{12}$ | $\nu_{12}$ |
| | 5.6466 TPa | 7.0800 TPa | 1.9445 TPa | 0.175 |
| PmPV | $E$ | $\nu$ | | |
| | 2.1 GPa | 0.34 | | |

**Table 3.** The variation of the uniaxial and biaxial buckling loads of FG-CNTRC spherical panel with respect to the volume fraction

| | $\frac{a}{R}$ | Type | $V^*_{CNT}$ | | |
|---|---|---|---|---|---|
| | | | 0.11 | 0.14 | 0.17 |
| Uniaxial (Sy = 0) | 0.5 | UD | 43.9742 | 50.6659 | 68.2309 |
| | | FG-A | 35.5999 | 41.0839 | 55.3723 |
| | | FG-V | 37.1185 | 42.5009 | 57.6141 |
| | | FG-X | 54.0226 | 62.2129 | 84.5242 |
| | | FG-O | 31.5429 | 36.0554 | 48.9213 |
| | 1 | UD | 74.8983 | 82.1657 | 117.3679 |
| | | FG-A | 67.1783 | 73.6256 | 106.1113 |
| | | FG-V | 68.7046 | 76.28927 | 107.1090 |
| | | FG-X | 83.6466 | 92.3473 | 132.0993 |
| | | FG-O | 60.6915 | 69.3809 | 94.2660 |
| Biaxial (Sy = 1) | 0.5 | UD | 14.4921 | 16.0402 | 22.6410 |
| | | FG-A | 12.3794 | 13.7310 | 19.5096 |
| | | FG-V | 13.7663 | 15.0657 | 21.5414 |
| | | FG-X | 16.6725 | 18.3550 | 26.4913 |
| | | FG-O | 11.9128 | 12.9863 | 18.4832 |
| | 1 | UD | 26.8439 | 28.5004 | 42.2729 |
| | | FG-A | 24.4204 | 26.3322 | 38.8705 |
| | | FG-V | 26.9896 | 28.8049 | 42.6349 |
| | | FG-X | 28.2086 | 30.2548 | 45.3212 |
| | | FG-O | 24.7161 | 26.3545 | 38.9797 |

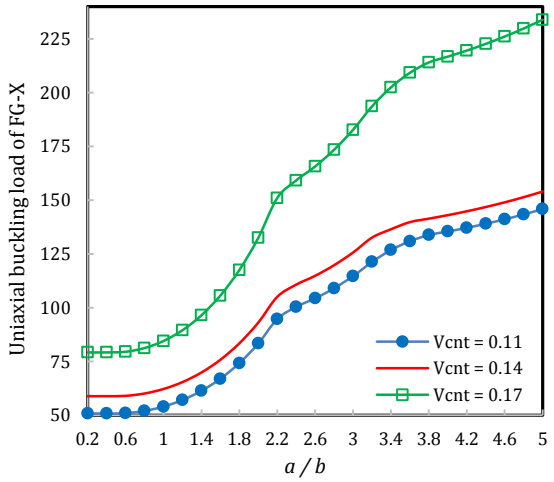


**Figure 3.**The influence of the volume fraction on the uniaxial buckling loads of FG-X spherical panel with respect to the aspect ratio

Furthermore, the analysis of static stability of UD and FG-CNTRC spherical panels reveals that FG-X and FG-O cases have the highest and lowest uniaxial and biaxial critical loads, respectively.

Fig. 6 illustratesthe effect of the aspect ratio on the percent change of the uniaxial buckling load for $V^*_{CNT}$ = 0.11, $h/a$ = 0.05 and $a/R$ = 0.5. It is shown that for FG-X spherical panel, with a decrease in the aspect ratio, the effectiveness of functionally graded distribution increases up to about 25 percent. In addition, it can be seen that for specific high aspect ratio FG-X panel with length to width ratio equal to 5, the effectiveness of functionally graded distribution has negligible value (about 3 percent). Furthermore, unlike the FG-X spherical panel, the other FG-CNTRC panels (FG-A, FG-V and FG-O) represent negative values for the percent change of buckling load. It physically means that the UD- CNTRC panel is more stable than FG-A, FG-V and FG-O nanocomposites. Hence, for the case of negative value, using the FG-distributions is not effective.

The influence of the side-to-radius ratio, $a/R$, on the non-dimensional uniaxial buckling load of the spherical nanocomposite panels is illustrated in Fig. 7. Here, we take $V^*_{CNT}$ = 0.11, $a/b$ = 1, $h/a$ = 0.05 and $S_y$ = 0. It reveals that the critical buckling load increases monotonically with the increase in the side-to-radius ratio. It should be noted that the similar trends for buckling of isotropic and functionally graded shallow spherical shells are presented in Ref. [30, 32]. Furthermore, it shows that FG-X and FG-O spherical panels are the most and the least stable nanocomposite panels among various kinds of the CNTRC spherical panels, respectively. It should be noticed that zero value of the side-to-radius ratio reveals the critical loads of CNTRC plate.

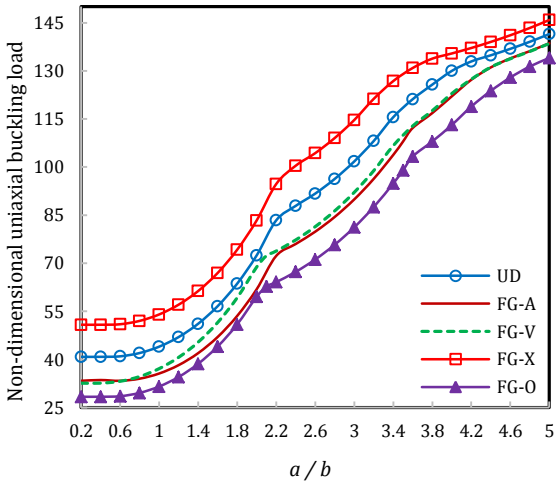


**Figure 4.** The variation of the uniaxial critical loads of the CNTRC spherical panel with respect to the aspect ratio

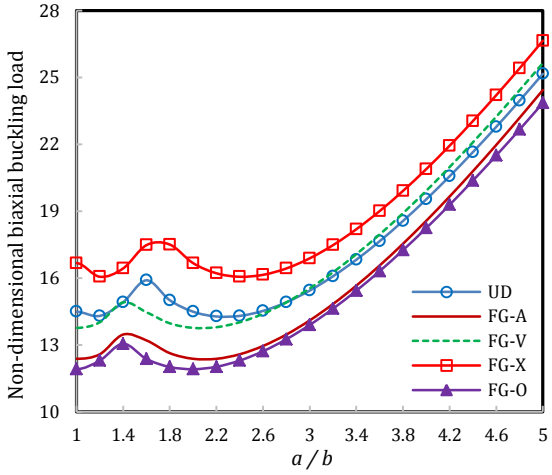


**Figure 5.** The effects of the aspect ratio on the biaxial buckling loads of the CNTRC spherical panel

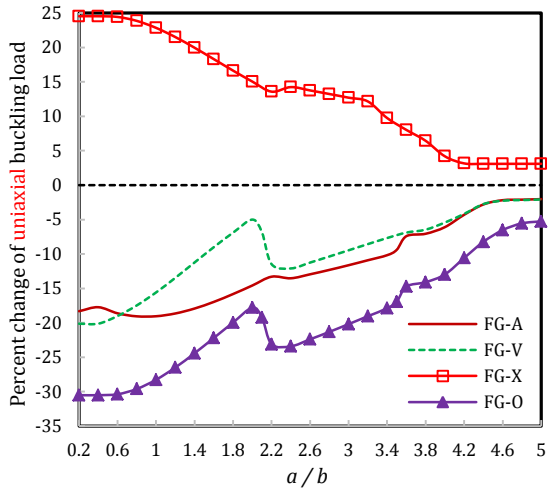


**Figure 6.** The influence of the aspect ratio on the percent change of uniaxial buckling load of FG-CNTRC spherical panel

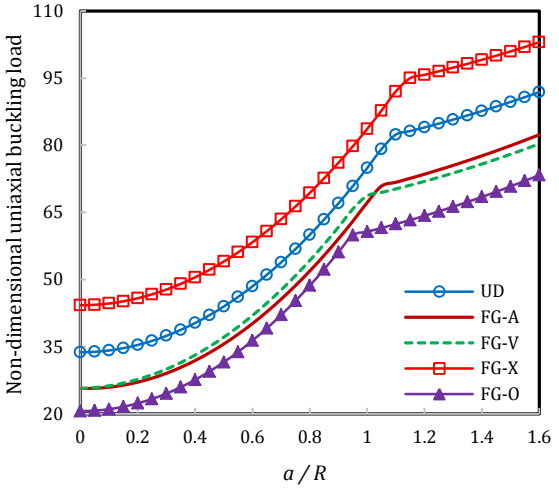


**Figure 7.** The effect of the side-to-radius ratio on the uniaxial critical loads of the CNTRC spherical panel

Uniaxial and biaxial buckling loads of the CNTRC spherical panels are compared with respect to the side-to-radius ratio in Fig. 8. For numerical calculationin this case, the same physical and geometrical properties, used in Fig. 7, are considered. Based on the anticipation, biaxial buckling loads of the CNTRC spherical panels are higher than uniaxial critical loads, for all values of side-to-radius ratio. Additionally, the distinction between uniaxial and biaxial critical compressive loads decreases with the decrease in the side-to-radius ratio.

The variations of uniaxial and biaxial buckling loads of UD-CNTRC with respect to aspect ratio and side-to-radius ratio are illustrated in Figs. 9 and 10, respectively. Here, we take $V^*_{CNT}$ = 0.11 and $h/a$ = 0.05. It is shown that with the increase in the aspect ratio and side-to-radius ratio, non-dimensional uniaxial buckling loads of the CNTRC panels increase.

In addition, for high aspect ratio CNTRC panels, negligible variation of the uniaxial buckling load with respect to the side-to-radius ratio is revealed. Furthermore, with the increase in the side-to-radius ratio, the non-dimensional biaxial buckling loads of CNTRC panels increase. However, according to the aforementioned results, the non-monotonic variation of the biaxial buckling load with respect to the aspect ratio is shown.

Figs. 11 and 12 reveal the variation of uniaxial and biaxial critical loads of UD and FG-CNTRC spherical panels with respect to the thickness ratio, $h/a$, respectively. In this study, we take $V^*_{CNT}$ = 0.11 $a/R$ = 0.5 and $a/b$ = 1. Here, to study the influences ofthe thickness ratio, the non-dimensional buckling load is redefined as what follows:

$$N_{cr} = \hat{N}_x \Big/ \left(E^m a\right) \tag{19}$$

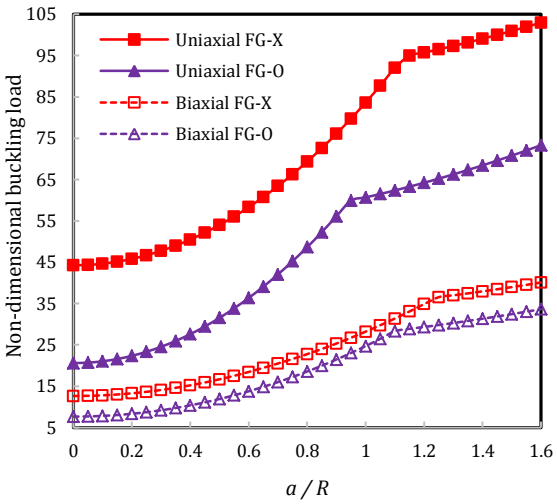


**Figure 8.** The variation of the uniaxial and biaxial critical loads of the CNTRC spherical panel with respect to the side-to-radius ratio

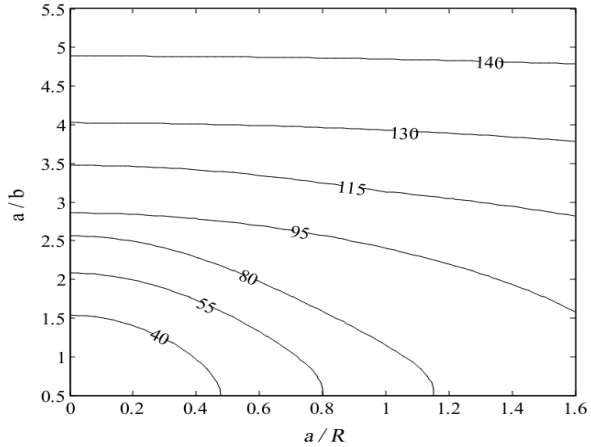


**Figure 9.** The contour plots of uniaxial critical loads of UD-CNTRC spherical panel with respect to the aspect ratio and side-to-radius ratio

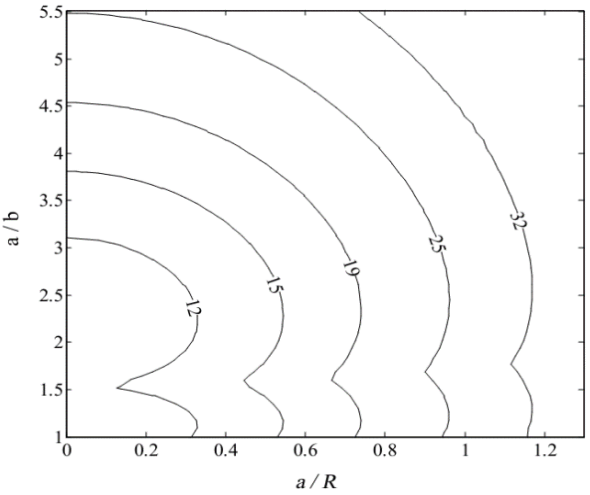


**Figure 10.** The contour plots of biaxial buckling loads of UD-CNTRC panel against the aspect ratio and side-to-radius ratio

In Figs. 11 and 12, it is revealed that with the increase in the thickness ratio, the stiffness of CNTRC panel increases and consequently, the uniaxial and biaxial critical loads increase. Note that the similar trend for buckling of nanocomposite plate is illustrated in Ref. [27]. Furthermore, the FG-X has the highest critical loads among various kinds of FG-CNTRC spherical panels. In addition, the static instability of CNTRC panels subjected to uniaxial buckling load occurs at higher compressive load than those subjected to biaxial buckling loads.

Additionally, the effect of the thickness ratio on the PCB of CNTRC panels is presented in Fig. 13. With the variation of the thickness ratio, PCB of FG-CNTRC spherical panels vary non-monotonically. For both thin and moderately thick FG-CNTRC spherical panels, the case of functionally graded distribution, FG-X, is effective enough in comparison with the uniform distribution.

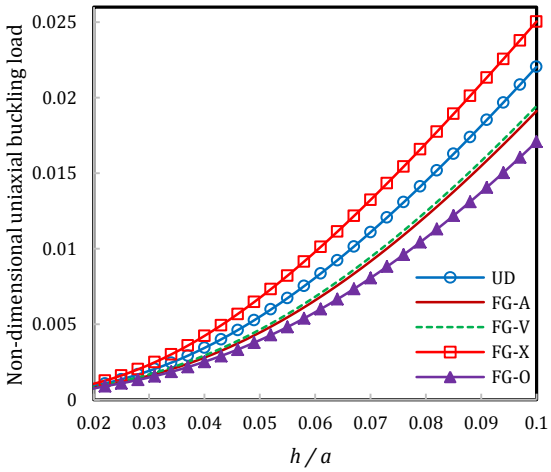


**Figure 11.** The variation of the uniaxial critical buckling load of CNTRC spherical panel with respect to the thickness ratio

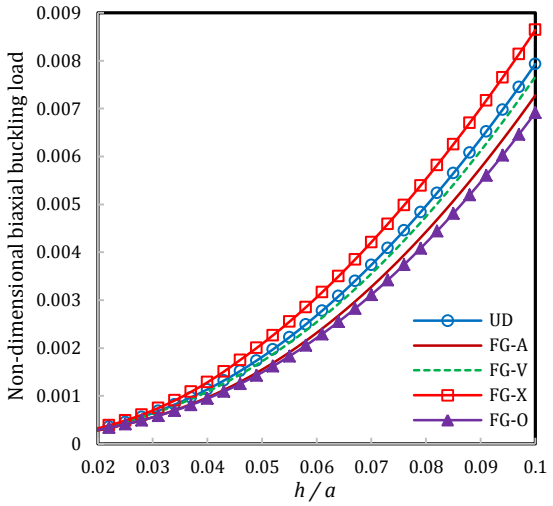


**Figure 12.** The change of the biaxial buckling load of CNTRC panel against the thickness ratio

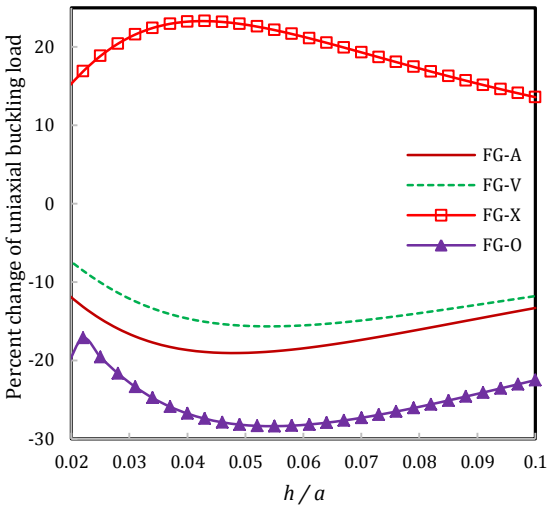


**Figure 13.** The effect of the thickness ratio on the percent change of the uniaxial buckling load

## 4. Conclusion

In this study, the first attempt to predict the critical biaxial and uniaxial compressive loads of uniform and functionally graded carbon nanotube-reinforced spherical composite panels was investigated. Utilizing the modified rule of mixture, the effective mechanical properties of theCNTRC panels were determined. Using first-order shear deformation theory, five complex and highly-coupled differential governing equations were derived. The present relations and procedure have been successfully verified by comparing the obtained results with those available in the literature. To study the buckling behavior of the CNTRC, the influences of volume fraction of CNTs, aspect ratio, thickness ratio and side-to-radius ratio were examined. Based on the numerical results, it is found that the non-dimensional uniaxial and biaxial critical buckling

loads increase with the increase in the volume fraction. By increasing thickness ratio and side-to-radius ratio, the uniaxial and biaxial critical loads increase. However, the non-dimensional biaxial buckling load changes non-monotonically versus the aspect ratio. Additionally, theFG-X and FG-O nanocomposites have the highest and lowest non-dimensional biaxial and uniaxialcritical loads, respectively. It is seen that the static instability of the CNTRC subjected to uniaxial critical load occurs at higher compressive load than those subjected to the biaxial buckling loads. Furthermore, the effectiveness of functionally graded distribution decreased, with the increase in the aspect ratio. For the thin FG-CNTRC spherical panelsas well as the moderately thick panels, the distribution of CNT in FG-X panel is effective enough in comparison with the uniform distribution.

Finally, it should be noted that the thermal effect can be included in the buckling of the FG-CNTRC panels. This would be an interesting issue for future studies.

## References


[1] Iijima S. Helical Microtubules of Graphitic Carbon. *Nature* 1991; 354: 56–58.

[2] Cadek M, Coleman JN, Barron V, Hedicke K, Blau WJ. Morphological and Mechanical Properties of Carbon-Nanotube-Reinforced Semicrystalline and Amorphous Polymer Composites. *Appl Phys Lett* 2002; 81: 5123–5125.

[3] ThostensonET, ChouTW. On The Elastic Properties of Carbon Nanotube-Based Composites: Modelling and Characterization. *J Phys D: Appl Phys* 2003; 36: 573–582.

[4] LauKT, GuC, GaoGH, LingHY, ReidSR. Stretching Process of Single and Multiwalled Carbon Nanotubes for Nanocomposite Applications. *Carbon* 2004; 42: 426–428.

[5] Coleman JN, Khan U, Blau WJ, Gunko YK. Small but Strong: A Review of the Mechanical Properties of Carbon Nanotube-Polymer Composites. *Carbon* 2006; 44: 1624–1652.

[6] Qian D, Dickey EC, Andrews R, Rantell T. Load Transfer and Deformation Mechanisms in Carbon Nanotube-Polystyrene Composites. *Appl Phys Lett* 2000; 76: 2868–2870.

[7] Ruan SL, Gao P, Yang XG, Yu TX. Toughening High Performance Ultrahigh Molecular Weight Polyethylene Using Multiwalled Carbon Nanotubes. *Polymer* 2003; 44: 5643–5654.

[8] Rafiee R, FirouzbakhtV.Predicting Young's Modulus of Aggregated Carbon Nanotube Reinforced Polymer, *Mech Adv Compos Struct* 2014; 1: 9–16.

[9] Mohammadimehr M, Rousta-Navi B, Ghorbanpour-Arani A.Biaxial Buckling and Bending of Smart Nanocomposite Plate Reinforced by CNTs Using Extended Mixture Rule Approach. *Mech Adv Compos Struct* 2014; 1: 17–26.

[10] Alibeigloo A. Elasticity Solution of Functionally Graded Carbon Nanotube Reinforced Composite CylindricalPanel. *Mech Adv Compos Struct* 2014; 1: 49–60.

[11] Tahouneh V, Eskandari-Jam J. A Semi-analytical Solution for 3-D Dynamic Analysis of Thick Continuously Graded Carbon Nanotube-Reinforced Annular Plates Resting on a Two-Parameter Elastic Foundation. *Mech Adv Compos Struct* 2014; 1: 113–130.

[12] ShenHS. Postbuckling of Nanotube-Reinforced Composite Cylindrical Shells in Thermal Environments, Part I: Axially-Loaded Shells. *Compos Struct* 2011; 93: 2096–2108.

[13] ShenHS.Postbuckling of Nanotube-Reinforced Composite Cylindrical Shells in Thermal Environments, Part II: Pressure-Loaded Shells. *Compos Struct* 2011; 93: 2496–503.

[14] ShenHS.Thermal Buckling and Postbuckling Behavior of Functionally Graded Carbon Nanotube-Reinforced Composite Cylindrical Shells. *Compos Part B-Eng* 2012; 43: 1030–1038.

[15] Shen HS, Xiang Y.Postbuckling of Nanotube-Reinforced Composite Cylindrical Shells under Combined Axial and Radial Mechanical Loads in Thermal Environment, *Compos Part B-Eng* 2013; 52: 311–322.

[16] Liew KM, Lei ZX, Yu JL, Zhang LW. Postbuckling of Carbon Nanotube-Reinforced Functionally Graded Cylindrical Panels under Axial Compression Using a Meshless Approach. *Comput Method Appl* 2014; 268: 1–17.

[17] Shen HS. Torsional Postbuckling of Nanotube-Reinforced Composite Cylindrical Shells in Thermal Environments. *Compos Struct* 2014; 116: 477–488.

[18] Shen HS, Xiang Y. Postbuckling of Axially Compressed Nanotube-Reinforced Composite Cylindrical Panels Resting on Elastic Foundations in Thermal Environments. *Compos Part B-Eng* 2014; 67: 50–61.

[19] JamJE, KianiY.Buckling of Pressurized Functionally Graded Carbon Nanotube Reinforced Conical Shells. *Compos Struct* 2015; 125: 586–595.

[20] RabaniBidgoli M, Karimi MS, GhorbanpourArani A. Nonlinear Vibration and Instability Analysis of Functionally Graded CNT-Reinforced Cylindrical Shells Conveying Viscous Fluid Resting on Orthotropic Pasternak Medium. *Mech Adv Mater Struct* 2016; 23: 819–831.

[21] Mohammadimehr M, RoustaNavi B, GhorbanpourArani A. Free Vibration of Viscoelastic Double-Bonded Polymeric Nanocomposite

Plates Reinforced by FG-Swcnts Using MSGT, Sinusoidal Shear Deformation Theory and Meshless Method. *Compos Struct* 2015; 131: 654–671.

[22] Mohammadimehr M, RoustaNavi B, GhorbanpourArani A. Modified Strain Gradient Reddy Rectangular Plate Model for Biaxial Buckling and Bending Analysis of Double-Coupled Piezoelectric Polymeric Nanocomposite Reinforced by FG-SWNT. *Compos Part B-Eng* 2016; 87: 132–148.

[23] Mohammadimehr M, Salemi M, RoustaNavi B. Bending, Buckling, and Free Vibration Analysis of MSGT Microcomposite Reddy Plate Reinforced by FG-Swcntswith Temperature-Dependent Material Properties under Hydro-Thermo-Mechanical Loadings Using DQM. *Compos Struct* 2016; 138: 361–380.

[24] Ghorbanpour Arani A, Jamali M, Mosayyebi M, Kolahchi R. Analytical Modeling of Wave Propagation in Viscoelastic Functionally Graded Carbon Nanotubes Reinforced Piezoelectric Microplate under Electro-Magnetic Field. *Mech Eng J Nano-Eng Nano-Sys*, Doi: 1740349915614046.

[25] Shen HS. Nonlinear Bending of Functionally Graded Carbon Nanotube-Reinforced Composite Plates in Thermal Environments. *Compos Struct* 2009; 91: 9–19.

[26] Fazelzadeh SA, Pouresmaeeli S, Ghavanloo E. Aeroelastic Characteristics of Functionally Graded CarbonNanotube-Reinforced Composite Plates undera Supersonic Flow. *Comput Methods Appl Mech Eng* 2015; 285: 714–729.

[27] Lei ZX, Liew KM, Yu JL. Buckling Analysis of Functionally Graded Carbon Nanotube-Reinforced Composite Plates Using the Element-Free Kp-Ritz Method. *Compos Struct* 2013; 98: 160–168.

[28] AmabiliM. **Nonlinear vibrations and stability of shells and plates**. Cambridge University Press; 2008.

[29] Kiani Y, Akbarzadeh AH, Chen ZT, Eslami MR. Static and Dynamic Analysis of an FGM Doubly Curved Panel Resting on the Pasternak-Type Elastic Foundation. *Compos Struct* 2012; 94: 2474–2484.

[30] MatsunagaH. Free Vibration and Stability of Functionally Graded Shallow Shells According to a2D Higher-Order Deformation Theory. *Compos Struct* 2008; 84: 132–146.

[31] Zhang LW, Lei ZX, Liew KM. An Element-Free IMLS-Ritz Framework for Buckling Analysis of FG-CNT Reinforced Composite Thick Plates Resting on Winkler Foundations. *Eng Anal Bound Elem* 2015; 58: 7–17.

[32] Matsunaga H. Vibration and Stability of Thick Simply Supported Shallow Shells Subjected to In-Plane Stresses. *J Sound Vib* 1999; 225: 41–60.